

Creation and consumption of free Si atoms at the growth front of a CaF monolayer on Si(111) 7×7

T. Nakayama*

The Institute of Physical and Chemical Research (RIKEN), 2-1 Hirosawa, Wako, Saitama 351-01, Japan

M. Aono

*The Institute of Physical and Chemical Research (RIKEN), 2-1 Hirosawa, Wako, Saitama 351-01, Japan
and Department of Precision Science and Technology, Osaka University, Suita, Osaka 565, Japan*

(Received 28 February 1997; revised manuscript received 8 September 1997)

Intrinsic defects in a CaF monolayer grown on a Si(111) 7×7 surface have been observed using a scanning tunneling microscope, and their locations with respect to the 7×7 substrate lattice before the growth of the CaF monolayer have been analyzed. We have found that the probability of the appearance of defects is smaller in unfaulted, dimer, faulted, and corner-hole regions of the 7×7 unit cell, in this order. These results are explained by considering the rearrangement of Si atoms from the 7×7 to 1×1 bulklike structure, which involves the creation and consumption of free Si atoms at the growth front of the CaF monolayer. The probability of the appearance of defects seems to be governed by the speed of the progress of the growth front of CaF, which is different in each of the four regions mentioned above. This mechanism also explains the shape of the CaF islands. [S0163-1829(98)05203-5]

I. INTRODUCTION

When growing thin films on semiconductor surfaces, a reduction of the number of defects in the films is a technological requirement.¹ In the case of calcium fluoride (CaF₂) on Si(111), which is an extensively studied system,² such defects are classified into two types. The first type is dislocations which result from the mismatch between the lattice constants of Si and CaF₂ (0.6% at room temperature). Although the CaF₂ film grows without dislocations up to a critical thickness, when it exceeds this thickness, a dislocation network starts to grow for strain relaxation,³ resulting in a two-dimensional structural modulation.⁴ The second type is point defects that are inevitably created at the interface even if the film is only one monolayer thick.^{5,6} Such defects seem to originate due to the growth mechanism of the monolayer [the first layer of CaF₂ on Si(111) has the composition of CaF (Ref. 7)] related to Si-atom rearrangement on the Si(111) 7×7 substrate.⁶ Elimination of these intrinsic defects is desired in creating nanoscale electronic devices which require films thinner than the critical thickness. In addition, it is of interest to qualify the atomic processes in detail in the initial stage of the growth of epitaxial films on Si(111) 7×7 in terms of energetics and kinetics.⁸ Up to now, the complexity of the Si(111) 7×7 structure⁹ has made it difficult to perform these kinds of investigations.

In this paper, we propose a mechanism for the formation of "intrinsic defects" in the growth of a CaF monolayer on Si(111) 7×7 , which involves the creation and consumption of "free" Si atoms at the growth front of the CaF monolayer, on the basis of scanning tunneling microscopy (STM) observations. The proposed mechanism has been derived from the analysis of the location of intrinsic defects with respect to the 7×7 substrate atomic lattice.

II. EXPERIMENTAL

A Si(111) 7×7 substrate was prepared by a procedure described elsewhere.⁶ The substrate was kept at 600 °C during the growth of a CaF layer,⁶ at a growth rate of about 0.15 ML per minute. The kinetic growth conditions used here resulted in the formation of a type-B chemisorbed CaF layer, in which Ca and F atoms occupy T_4 and H_3 sites, respectively.^{7,10} The scanning tunneling microscope was operated at room temperature in an ultrahigh vacuum better than 1.3×10^{-8} Pa, with an electrochemically etched tungsten tip.

The sample was prepared such that the 7×7 and CaF regions appeared simultaneously. This was essential in our experiments because the use of a "clean" tip that correctly gives a metallic current-voltage dependence for the 7×7 region¹¹ was necessary. Using such a clean tip, we were able to obtain STM images with atomic resolution reproducibly for both the 7×7 and CaF regions.

III. RESULTS AND DISCUSSION

A. Defect registration

Figure 1 shows an example of STM images used for the registration of intrinsic defects. The upper and lower parts of Fig. 1 correspond to the CaF and 7×7 regions, respectively. This image was obtained under a filled-state imaging condition [a sample bias (V_s) of -1.5 V, a tunnel current (I_t) of 500 pA]. In the CaF region, the intrinsic defects are observed (some of which are indicated by arrows), in addition to very shallow 1×1 periodic depressions which coincide with the periodicity of the CaF structure. The intrinsic defects are classified into two types.⁶ One is small defects which have a unique triangular shape, the center of which is always located at an H_3 site in the Si(111) 1×1 lattice at the interface.⁶ The other is large defects of various shapes. At

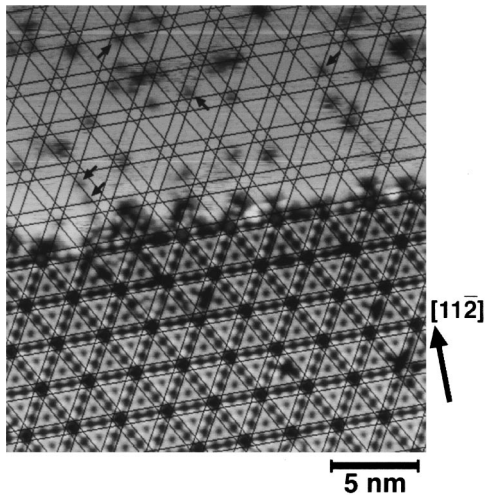


FIG. 1. STM image of the boundary between the Si(111) 7×7 and CaF/Si(111) structures. In the CaF region, defects are observed as dark spots. Some of the elemental defects are indicated by arrows. The superimposed mesh represents the 7×7 structure.

the edges of these large defects, however, traces of the small defect (part of the triangle) are observed in most cases, indicating that the large defects are complexes of the small ones. Hereafter, we refer to the small and large defects as elemental and complex defects, respectively.

As we already reported,⁶ one elemental defect seems to involve one or three Si atoms, and we have not been able to determine the atomic structure of the elemental defect in detail. The incorporated Si atom or atoms will be located on the H_3 or T_4 site in the Si(111) 1×1 lattice, depending on whether the elemental defect involves one or three Si atoms, respectively. Although a Si adatom on the Si(111) 7×7 surface is more stable at the T_4 site than at the H_3 site,¹¹⁻¹³ this may not be the case when Ca-Si or F-Si bonding¹⁰ plays an important role in the incorporation of Si atoms into the CaF monolayer. In the following discussion, the atomic structure of the elemental defect is not considered, and only the number of Si atoms in one elemental defect is taken into account.

In order to see positional correlations of these elemental and complex defects with the 7×7 structure before the growth of CaF, a mesh has been superimposed on the STM image in Fig. 1. In Fig. 2(a), the mesh in Fig. 1 is shown with reference to the 7×7 structure. We divide the 7×7 structure into four regions, i.e., unfaulted (U), dimer (D), faulted (F), and corner-hole (C) regions, as indicated in Fig. 2(a). In Fig. 2(b), the positions of H_3 sites (crosses) and the interfacial Si atoms (open circles) after the growth of CaF are shown with respect to the mesh in Fig. 2(a).

Figures 3(a) and 3(b) show STM images of the elemental defects on a magnified scale, together with the mesh described above. The positions of the elemental defects involved in these defects are depicted in Figs. 3(c) and 3(d), where the open circles show the interfacial Si atoms. The elemental defects observed in Figs. 3(a) and 3(b) are located in C and D regions, respectively. This kind of registration was performed over many CaF regions, with the total area corresponding to 462 7×7 unit cells, which contained 196 elemental and 132 complex defects. The number fraction of

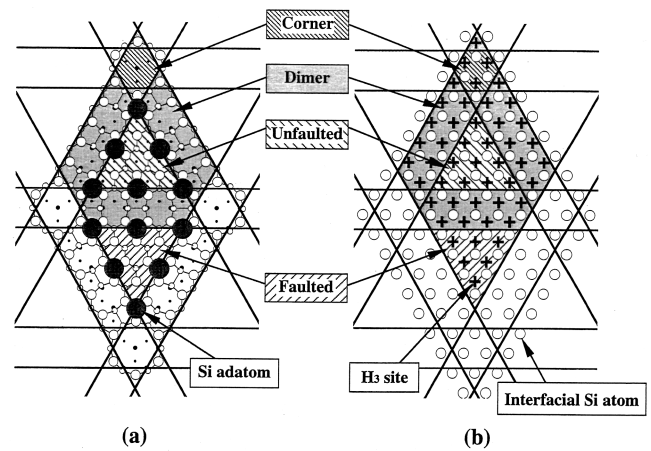


FIG. 2. (a) The mesh used in Fig. 1. This mesh divides the Si(111) 7×7 structure into four regions, i.e., unfaulted, dimer, faulted, and corner-hole regions. (b) Positions of the interfacial Si atoms (open circles) after the growth of CaF with respect to the mesh shown in (a). Crosses in (b) indicate H_3 sites of the Si substrate.

isolated elemental defects were 60%, and a single complex defect had an area 6.0 times larger than that of a single elemental defect on average.

When counting the number of elemental defects in U , D , F , and C regions, the complex defects must be decomposed into the elemental defects. This can be done manually for most complex defects smaller than about the average size. However, this decomposition is difficult for larger complex defects, because they seem to have unknown extended structures. Therefore, we estimate the number of elemental defects in such a large defect from its area.

When we denote the average number of the elemental defects in a complex defect by \bar{n} , the relation between the

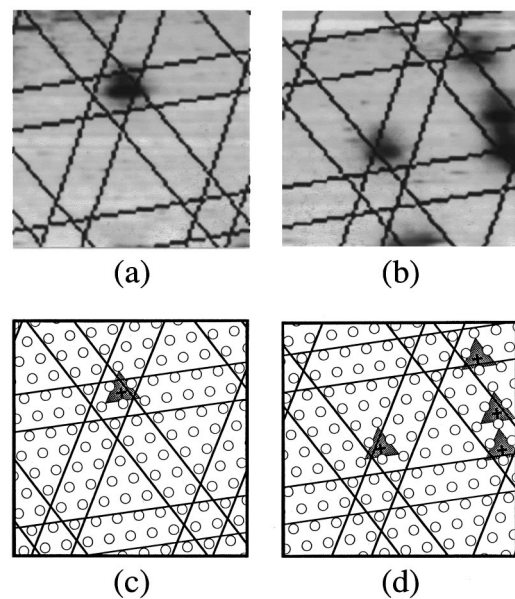


FIG. 3. (a) and (b) magnified STM images of elemental defects. (c) and (d) schematic diagrams corresponding to (a) and (b), respectively. The defects in (a) and (b) are classified as belonging to C and D regions, respectively.

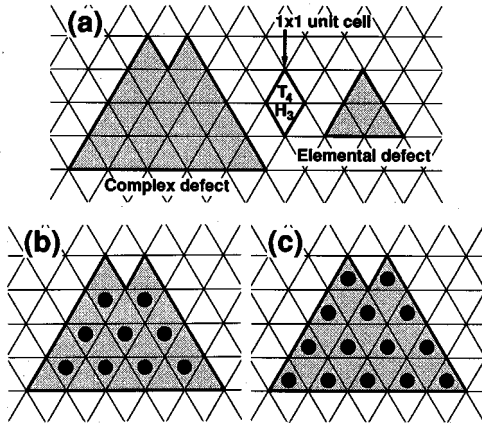


FIG. 4. Number of Si atoms in a complex defect. (a) A complex defect which has an area $\frac{23}{4}$ times larger than the elemental defect is shown. (b) and (c) correspond to the cases that the complex defect is composed of elemental defects with single and three Si atoms, respectively.

total number of elemental defects (N_d) and the number of isolated elemental defects (n_d) is expressed as below, since the number fraction of elemental defects is 60%:

$$N_d = \left(\frac{1-0.60}{0.60} \times n_d \right) \times \bar{n} + n_d = \left(\frac{2\bar{n}}{3} + 1 \right) \times n_d \equiv \alpha \times n_d. \quad (1)$$

Let us consider the complex defect shown in Fig. 4(a), which has an area $\frac{23}{4}$ times larger than that of the elemental defect, as an example. In the case of the elemental defect with a single Si atom, the number of Si atoms in this complex defect is nine [see Fig. 4(b)], which corresponds to 9 elemental defects. In the case of the elemental defect with three Si atoms, the number is 14 [see Fig. 4(c)], which corresponds to $\frac{14}{3} = 4.7$ elemental defects. We have considered possible shapes for many sizes of complex defects, and calculated the average number of Si atoms involved in the defects. The average size of complex defects was 6.0 times larger than the size of the elemental defect, as already described, and the number of elemental defects in one complex defect (\bar{n}) was estimated to be 9.5 or 4.8 on average, depending on the number of Si atoms in one elemental defect. Therefore, α is calculated to be 7.3 ($\bar{n} = 9.5$, one Si atom in one elemental defect) or 4.2 ($\bar{n} = 4.8$, three Si atoms in one elemental defect) using Eq. (1).

Using Eq. (1) and the values for α , the complex defects can be statistically decomposed into elemental defects. However, the positional correlations between elemental defects involved in a complex defect and the 7×7 structure before the growth of CaF are not derived in this case. Then we assume that the positional correlation of such elemental defects is identical to that of the isolated elemental defects which are clearly correlated to the 7×7 structure, as shown in Figs. 3(a) and 3(b).

The numbers of elemental defects, N_d , in U , D , F , and C regions were estimated from the numbers of isolated elemental defects, n_d , in the respective regions. Using the number of H_3 sites (N_H) per 7×7 unit cell, which is readily obtained from Figs. 2(b) and 2(c), we can derive the probability of the appearance of defects per H_3 site (P) by calculating $P = N_d / (462 \times N_H)$. In Table I, N_d , N_H , and P in U , D , F , and C regions are given for $\alpha = 7.3$ and 4.2. P is smaller in U , D , F , and C regions in this order. The C region exhibits a much larger P (12–20 %) compared with the other three regions (<7.4%).

B. Mechanism of defect formation

The growth of the CaF monolayer on the Si(111) 7×7 substrate requires rearrangement of Si atoms in the top three layers of the 7×7 structure into the two outermost Si layers, with a bulklike 1×1 structure at the interface.⁶ During this structural change, the Si adatoms in the first layer [filled circles in Fig. 2(a)] are ejected from their positions and the Si atoms in the second and third layers [large and small open circles, respectively, in Fig. 2(a)] are rearranged. Since the number of Si atoms in the second and third layers of the 7×7 structure is smaller than that in the two outermost layers in the 1×1 bulklike structure, a certain number of Si atoms is required to complete the rearrangement. We therefore consider the process in the following three steps: (1) the ejection of the Si adatoms in the first layer, (2) the rearrangement of the Si atoms in the second and third layers, and (3) the supply of the ejected Si atoms.

Figures 5(a)–5(f) explain how the above three steps take place during the rearrangement of Si atoms. Figures 5(a) and 5(b) show side and top views of the 7×7 structure, respectively, and step (1) results in the structure presented in Fig. 5(c). The Si atoms with arrows in Fig. 5(c) must be displaced [step (2)] in order to proceed rearranging the 7×7 structure into the 1×1 structure. The direction of the atomic displacement indicated by the arrows is one of the possibilities. As a result of this displacement, there are eight atomic vacancies

TABLE I. Results of registration of elemental defects.

$(\alpha = 7.3)$	Unfaulted (U)	Dimer (D)	Faulted (F)	Corner hole (C)
N_d	204 ± 23	745 ± 82	204 ± 23	277 ± 30
N_H	10	30	6	3
P	0.044 ± 0.005	0.054 ± 0.006	0.074 ± 0.008	0.200 ± 0.022
$(\alpha = 4.2)$				
N_d	118 ± 13	428 ± 47	118 ± 13	159 ± 17
N_H	10	30	6	3
P	0.026 ± 0.003	0.031 ± 0.003	0.043 ± 0.005	0.115 ± 0.013

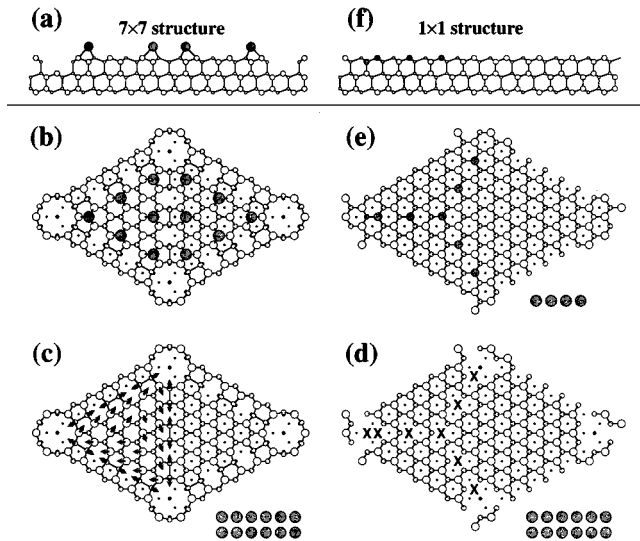


FIG. 5. Atomic rearrangement of the Si(111)7 \times 7 structure. The 7 \times 7 structure [(a) and (b)] is rearranged into the 1 \times 1 structure [(e) and (f)] through three steps (1), (2), and (3) which correspond to the structural changes from (b) to (c), (c) to (d), and (d) to (e), respectively.

per 7 \times 7 unit area, as indicated by crossings in Fig. 5(d). Finally, as shown in Figs. 5(e) and 5(f), these vacancies are repaired by the Si atoms ejected at the beginning of the rearrangement [step (3)].

Table II is a “yes-no” list showing which of the steps mentioned above are required to rearrange *U*, *D*, *F*, and *C* regions. In the *C* region, there are no Si adatoms at the beginning [see Fig. 2(a)]. Nevertheless, step (1) is required because this region cannot be rearranged into 1 \times 1 without ejection of surrounding Si adatoms. In addition, steps (2) and (3) are required in this region. Also, in the *F* region, not only step (1) but also steps (2) and (3) are required, although step (2) in this region occurs much more easily than in the *C* region. In the *D* region, only steps (1) and (2) are required, and step (3) is unnecessary. Finally, the *U* region requires only step (1); steps (2) and (3) are unnecessary. We therefore conclude that the ease of rearrangement of Si atoms increases in *U*, *D*, *F*, and *C* regions in this order. The present argument is, of course, too simplified, since each step is not necessarily independent of other steps and the existence of Ca and F atoms must be taken into consideration. However, this simple argument can explain our experimental results summarized in Table I. That is, the probability of the appearance of defects, *P*, is smaller in *U*, *D*, *F*, and *C* regions in this order.

From these results, one may think that the defects are created as a result of incomplete rearrangement of Si atoms into the 1 \times 1 bulklike structure. However, this is not the

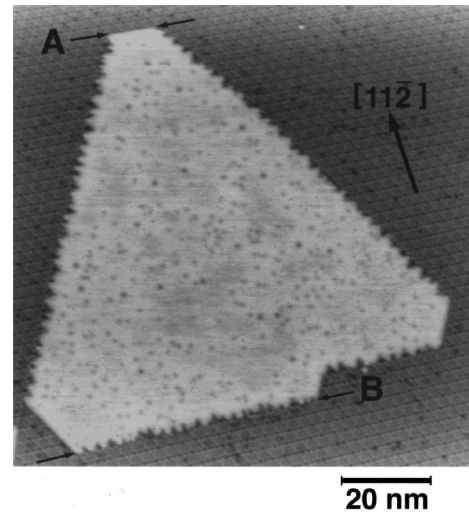


FIG. 6. STM image of a CaF island grown on a Si(111)7 \times 7 substrate. The island is surrounded by two types of growth fronts, A and B. Note that the A-type growth front is smooth and short, while the B-type growth front is rough and long.

case judging from the following two experimental findings:⁶ (i) the density of elemental defects agrees well with that of the excess Si atoms created during the growth of CaF, and (ii) all the elemental defects are the same in shape, size, orientation, and site. Therefore, we propose the following mechanism for defect creation.

At the growth front of the CaF monolayer, the Si adatoms of the 7 \times 7 structure are ejected and become free Si atoms near the growth front. Although most of the free Si atoms are used to complete the rearrangement into the 1 \times 1 structure, excess Si atoms still exist. They are captured at the CaF/Si(111) interface, where the rearrangement into the 1 \times 1 structure has already been completed, and result in the defects. It should be noted that the speed of the progress of the growth front of CaF is reduced in a region where the rearrangement of Si atoms is difficult, or the growth front stays in such a region for a longer time. Therefore, the probability of the capture of the excess Si atoms increases in such a region, resulting in an increase of *P*, as seen in Table I. This mechanism can explain all the experimental results in the present and previous work.⁶

C. Shapes of CaF islands

What we discussed in Sec. III B is also consistent with the shapes of the CaF islands, an example of which is shown in Fig. 6. The CaF islands have two types of growth front, A and B. The A-type growth front is smooth, while the B-type growth front is rough, the former being shorter than the latter. The A-type growth front is always in the *C* region, while the B-type growth front is in the front of the *C* region.

TABLE II. Requirements for rearranging the 7 \times 7 structure.

	Unfaulted (<i>U</i>)	Dimer (<i>D</i>)	Faulted (<i>F</i>)	Corner-hole (<i>C</i>)
(1) Ejection of Si adatoms	Yes	Yes	Yes	Yes
(2) Rearrangement of Si atoms	No	Yes	Yes	Yes
(3) Supply of ejected Si atoms	No	No	Yes	Yes

In order for the *A*-type growth front to move forward, the rearrangement of Si atoms occurs first in the *U* region, then in the *F* region, and finally in the *C* region ($U \rightarrow F \rightarrow C$). For the *B*-type growth front, it occurs first in the *C* region, then in the *F* region, and finally in the *U* region ($C \rightarrow F \rightarrow U$). Since the rearrangement in the *D* region is common to both cases, it is omitted for simplicity. These different sequences of the rearrangement of Si atoms result in different densities of the free Si atoms near the two growth fronts, causing the different edge shapes (smooth and rough) seen in Fig. 6, as follows.

In the case of the *A*-type growth front, the ejected Si adatoms in the *U* region are kept free until the growth front starts to rearrange Si atoms in the *F* region into the 1×1 bulklike structure. In the case of the *B*-type growth front, the free Si atoms are required to rearrange Si atoms in the *C* region in the first step, but they are not created yet. Therefore the *B*-type growth front moves forward to the *F* region, as if the growth front avoids the *C* region. This is why the *B*-type growth front is rougher than the *A*-type growth front. Moreover, the *F* region itself requires free Si atoms, so some of the created free Si atoms are immediately used there. As a result, the density of the free Si atoms near the *B*-type growth front is lower than that near the *A*-type growth front when they are required to complete the rearrangement of Si

atoms into the 1×1 bulklike structure. Therefore, the *A*-type growth front moves faster than the *B*-type growth front, resulting in elongation of the *B*-type growth front.

IV. SUMMARY

We have proposed a mechanism for the formation of intrinsic defects in the growth of a CaF monolayer on the Si(111) 7×7 substrate. At the growth front of the CaF monolayer, free Si atoms are created in the process of the rearrangement of Si atoms from the 7×7 structure to the 1×1 bulklike structure. Most of these Si atoms are used to complete the rearrangement, but the rest of them form intrinsic defects. The probability of the appearance of defects varies according to the regions in the 7×7 structure, indicating that the speed of the progress of the growth front of the CaF monolayer depends on its location. This mechanism is consistent with the present and previous experimental results. In addition, it can explain the features of the edges of the CaF islands.

ACKNOWLEDGMENTS

This work was partially supported by the Program of Core Research for Evolutional Science and Technology (CREST), Japan Science and Technology Corporation.

*Author to whom correspondence should be addressed. Electronic address: tomonobu@postman.riken.go.jp

¹S. Shinharoy, *Thin Solid Films* **187**, 231 (1990).

²M. Sugiyama and M. Oshima, *Microelectron. J.* **27**, 361 (1996).

³R. M. Tromp, F. K. LeGoues, and M. C. Reuter, *Phys. Rev. Lett.* **74**, 2706 (1995).

⁴K. G. Huang, J. Zegenhagen, J. M. Phillips, and J. R. Patel, *Phys. Rev. Lett.* **72**, 2430 (1994).

⁵Ph. Avouris and R. Wolkow, *Appl. Phys. Lett.* **55**, 1074 (1989).

⁶T. Nakayama, M. Katayama, G. Selva, and M. Aono, *Phys. Rev. Lett.* **72**, 1718 (1994).

⁷R. M. Tromp and M. C. Reuter, *Phys. Rev. Lett.* **61**, 1756 (1988).

⁸J. A. Venables, J. S. Drucker, and G. Raynerd, in *Mechanisms of Heteroepitaxial Growth*, edited by M. F. Chisholm, R. Hull, L. J. Schowalter, and B. J. Garrison, MRS Symposia Proceedings No. 263 (Materials Research Society, Pittsburgh, 1992), p. 3.

⁹K. Takayanagi, Y. Tanishiro, M. Takahashi, and S. Takahashi, *J. Vac. Sci. Technol. A* **3**, 1502 (1985).

¹⁰J. D. Denlinger, E. Rotenberg, U. Hessinger, M. Leskovar, and M. A. Olmstead, *Phys. Rev. B* **51**, 5352 (1995).

¹¹Ph. Avouris and R. Wolkow, *Phys. Rev. B* **39**, 5091 (1989).

¹²Y.-N. Yang and E. D. Williams, *Phys. Rev. Lett.* **72**, 1862 (1994).

¹³T. Nakayama, T. Eguchi, and M. Aono, *Surf. Sci.* **320**, L101 (1994).